Structural Studies of HIV-1 Gag p6ct and Its Interaction with Vpr Determined by Solution Nuclear Magnetic Resonance[†,‡]

Gilmar F. Salgado,*[,§,||] Rodrigue Marquant,[§] Alexander Vogel,[⊥] Isabel D. Alves,[#] Scott E. Feller,[⊥] Nelly Morellet,[§] and Serge Bouaziz*[,§]

Unité de Pharmacologie Chimique et Génétique, Inserm U640, CNRS UMR8151, UFR des Sciences Pharmaceutiques et Biologiques, 4, avenue de l'Observatoire, 75270 Paris Cedex 06, France, Department of Chemistry, Wabash College, 301 West Wabash Avenue, Crawfordsville, Indiana 47933, and [1]UPMC Univ Paris 06, UMR 7613, Synthèse, Structure et Fonction de Molécules Bioactives, FR 2769, and CNRS, UMR 7613, F-75005 Paris, France

Received September 20, 2008; Revised Manuscript Received January 3, 2009

ABSTRACT: The ability of human immunodeficiency virus type 1 (HIV-1) to egress from human cells by budding with the cell membrane remains a complex phenomenon of unclear steps. HIV-1 viral protein R (Vpr) incorporation in sorting virions relies greatly on the interaction with the group-specific antigen (Gag) C-terminal region, which encompasses protein p6. The complete role of p6 is still undetermined; however, it is thought that p6 interacts with protein core elements from the endosomal sorting complex ESCRT-1, known to sort ubiquitinated cargo into multivesicular bodies (MVB). The three-dimensional structure of the p6 C-terminus (p6ct) comprising amino acids 32−52, determined in this study using NMR methods, includes the region thought to interact with Vpr, i.e., the LXXLF sequence. Here we present new results indicating that the region which interacts with Vpr is the ELY[36] sequence, in the same region where mutational studies revealed that replacing Y36 with a phenylalanine would increase the infectivity of virions by 300-fold. The interaction of Vpr with an egg PC bilayer in the presence of p6ct measured by plasmon waveguide resonance (PWR) is ∼0.8 μM, ∼100 times stronger in the absence of p6ct. Our results suggests an interaction based on an ELYP[37] sequence bearing similarities with recently published results, which elegantly demonstrated that the HIV-1 Gag LYPx$_n$LxxL motif interacts with Alix 364−702. Moreover, we performed a 60 ns molecular dynamics (MD) simulation of p6ct in DPC micelles. The MD results, supported by differential scanning calorimetry measurements in DMPC, show that p6ct adsorbs onto the DPC micelle surface by adopting a rather stable α-helix. Our results provide insights regarding the HIV-1 virion sorting mechanism, specifically concerning the interaction between p6 and Vpr. We also suggest that Gag p6 may adsorb onto the surface of membranes during the sorting process, a property so far only attributed to the N-terminal portion of Gag matrix (MA), which is myristylated. The implications of such a novel event provide an alternative direction toward understanding the assembly and escape mechanisms of virions, which have been undetected so far.

Complete knowledge of the functional activity of human immunodeficiency virus type 1 (HIV-1)[1] proteins is a necessary daunting task. Despite intensive efforts, the process of virus assembly and budding is still undetermined. The multifunctional Gag p6 is a small 5 kDa protein consisting of 52 amino acids and is one of the seven HIV-1 Gag polyprotein Pr55 aspartic-protease cleavage byproducts. This process occurs after integration of the viral core particle into the cell cytoplasm. Other byproduct proteins include the matrix (MA), capsid (CA), and nucleocapsid (NC) proteins, as well as two spacer peptides, SP1 and SP2, located between CA and NC and between NC and p6, respectively. As

[†] This work was supported by the French Agency for AIDS Research (ANRS) and by Sidaction (Ensemble contre le SIDA). A.V. was the recipient of a postdoctoral scholarship from the Deutsche Forschungsgemeinschaft (VO1523/1-1). G.F.S. was supported by a postdoctoral fellowship from the Fundação para a Ciência e Tecnologia (SFRH/BPD/34153/2006). S.E.F. thanks the NSF and NIH for support through Grants MCB-0543124 and PHS 2 PN2 EY016570B, respectively.

[‡] The coordinates of the last 10 structures (in 1 ns increments) from the 60 ns CHARMM MD simulation started with the NMR-derived conformer of p6ct were deposited at the BioMagResBank (BMRB) as entry 15799, and the NMR-derived coordinates have been deposited as entry 15957.

* To whom correspondence should be addressed. E-mail: gilmar.salgado@ens.fr or serge.bouaziz@univ-paris5.fr. Phone: +33 1 53 73 95 78. Fax: +33 1 44 32 33 97.

[§] CNRS UMR8151.

[||] Current address: Département de Chimie, Ecole Normale Supérieure, CNRS, UMR 8642, 24 rue Lhomond, 75231 Paris cedex 05, France.

[⊥] Wabash College.

[#] UMR 7613.

[1] Abbreviations: ARIA, Ambiguous Restraints for Iterative Assignment; CHARMM, Chemistry at HARvard Macromolecular Mechanics; CD, circular dichroism; DMPC, dimyristoylphosphatidylcholine; GAG, group-specific antigen; HIV-1, human immunodeficiency virus type 1; HOBt/DCC, hydroxybenzotriazole/*N*,*N*′-dicyclohexylcarbodiimide; DPC-d_{38}, perdeuterated dodecylphosphocholine; DSC, differential scanning calorimetry; HPLC, high-performance liquid chromatography; MD, molecular dynamics; MVB, multivesicular bodies; NMR, nuclear magnetic resonance; NOE, nuclear Overhauser effect; NOESY, NOE spectroscopy; egg PC, egg phosphatidylcholine; PWR, plasmon waveguide resonance; TFA, trifluoroacetic acid; TFE, 2,2,2-trifluoroethanol; TOCSY, total correlation spectroscopy; WATERGATE, WATER suppression by GrAdient Tailored Exicitation.

10.1021/bi801794v CCC: $40.75
Published on Web 03/02/2009

observed and broadly accepted, the function of p6 seems to be mainly associated with an important scaffolding step during the HIV life cycle, i.e., assisting the assembly and packaging of viral particles, in particular Vpr, during their exit from infected cells (*1–3*). There are several factors known to influence virus budding and may include ionic strength conditions, plasma membrane cholesterol content, glycoprotein palmitoylation, membrane lateral protein−protein interactions, and protein−protein interactions between assembled intracellular proteins (*4*). In the case of Gag p6, the focus has been almost exclusively on protein−protein interactions and marginally discussed as a possible target for cellular membranes. Overall, the functions of Gag p6 in infected cells are not clear, and the mechanism of action in virion packaging is almost totally unknown. This is particularly evident in the lack of consensus concerning the amino acid composition of the domain implicated in the tasks mentioned above, or even the number of partners with which it might interact once inside the infected cell. The PTAP sequence represents such an example. The sequence, located at the N-terminus and also termed the late (L) domain, is associated with late sorting processes common to several viruses which use some sort of cellular membrane budding process where the host cellular membrane is severed upon assembly of virions (*5*). Nevertheless, the mechanism by which the PTAP region participates in viral maturation is far from clear; however, there are a few complementary studies which do show that residues 32−45, containing the LXXLF motif, are used as an anchor for cellular factors responsible for vesicular sorting (*6*). This region is the same thought to contain key amino acids responsible for the association with Vpr. Studies that present contradictory results claiming that the sequence motif necessary for virion packaging is located in the $FRFG^{18}$ amino acid region and not in the $LXXLF^{45}$ motif also exist (*7*). Several other interesting properties have been associated with p6, such as ubiquitination, phosphorylation of T23 (*8*), and the HIV-1 protease cleavage of the $KELY^{36}$ motif in the C-terminal region of p6 (p6ct). An important mutational study concerning Y36F showed a 300-fold increase in infectivity compared to that of the wild-type sequence (*9*). One distinctive feature in the HIV life cycle is the fact that Gag lacking p6 produces virions with a much smaller diameter of only 25−30 nm compared to 100−150 nm particles when it is assembled in vivo (*10*). There is also some evidence that the p6 $YPXL^{39}$ L domain-type sequence forms a ternary complex with AIP1/Alix and ESCRT-I proteins and is sufficient to trigger the formation of an endosomal sorting complex (ESCRT-III) required for complex transport on endosomal membranes (*11*). The large number of different processes known to start upon infection with HIV where p6 is thought to be implicated far surpasses the objectives of this work and can be better reviewed elsewhere (*12, 13*). Given the importance of such peptides, with a broad range of activities and an unclear structure−action relationship, knowledge of the structure and, most importantly, the interacting molecular constituents seems crucial for a better understanding of the events related to inclusion of Vpr in virions.

The objectives of this study are to evaluate the molecular characteristics bridging both Gag P6 and Vpr, using mainly solution state NMR methods employing samples without organic solvents, which may diminish or misguide the forces such as soft hydrophobic interactions or hydrogen bonding, presumably of extreme importance in such interactions. In this study, we present the NMR solution structure of the C-terminus of p6 (p6ct), comprising residues 32−52, in perdeuterated dodecylphosphocholine (DPC-d_{38}) micelles. The choice of DPC micelles comes naturally since the zwitterionic phosphatidylcholine headgroup of DPC is the same found in many biological membrane constituents such as palmitoyloleoylphosphatidylcholine (POPC). DPC, as well as sodium dodecyl sulfate (SDS), forms small micelles comprising 60−100 molecules (*14*) that rapidly tumble in solution on the NMR time scale (microseconds or faster) and have a critical micellar concentration of ~1.1 mM. The micelles are stable over a wide range of temperatures and pH, which is important for biological samples and been extensively employed together with NMR methods to study structure and dynamics of membrane-bound proteins (*15–18*). The three-dimensional structure calculations made use of classical distance geometry methods based on NOE cross-peak volumes, which were then converted to interproton distances. The peptide exhibits a similar secondary structure folding pattern as measured by circular dichroism (CD), both in 2,2,2-trifluoroethanol (TFE-50%) and in DPC (1:100 molar ratio). This is contrasted by the two-dimensional $^1H-^1H$ NMR spectra which exhibit different cross-peak patterns and chemical shift values. DPC micelles may play a chaperone role, assisting in p6ct structure formation, otherwise not possible in H_2O. This observation raises interesting questions regarding the potential role of DPC molecules (and consequently cellular membranes) interacting with p6 and folding it. The characteristics of the hydrophobic tail in p6 (P37−Q52) was modestly addressed (*9*), and unfortunately, the subject has not been further investigated. Previous NMR results using Gag p6 were based on high concentrations of organic solvents (*36*), which may explain some of the differences observed in this study. Additionally, we conducted a MD simulation of p6ct in a DPC micelle, which enabled us to refine the NMR structure in an explicit solvent/detergent system and improve our understanding of the peptide location together with the micelle structure. The MD results support the NMR structure in which p6ct forms an α-helix and seems to be adsorbed to the micelle surface in a stable manner, with most hydrophobic residue side chains embedded in the micelle interior while amino acids crucial for interaction with Vpr are on the surface of the micelle and thereby easily accessible to any interaction partner.

EXPERIMENTAL PROCEDURES

Materials. DPC-d_{38} (98.5%), TFE-d_3, and deuterium oxide were purchased from Eurisotop. Unless otherwise cited, all DPC used was perdeuterated DPC-d_{38}. Egg phosphatidylcholine (egg PC) and dimyristoylphosphatidylcholine (DMPC) were purchased from Avanti Lipids.

Peptide Synthesis. The 21-amino acid C-terminally truncated p6 peptide (p6ct) was produced by automated solid phase synthesis using a small scale Fmoc strategy on an ABI431A (Applied Biosystem) synthesizer. HMP resin (1.14 mmol/g) and amino acids were purchased from Applied Biosystems. Peptide elongation occurred by using protected amino acids coupled to activation by hydroxybenzotriazole/*N*,*N*′-dicyclohexylcarbodiimide (HOBt/DCC), leading to 210

mg of crude extract. The resulting mixture was purified by reverse phase HPLC (C18 column, 300 Å, 5 μm, 250 mm $\times$ 10 mm, Vydac) using a H_2O/0.05% TFA mixture (solvent A) and acetonitrile (solvent B) as the mobile phase. A 15 to 50% linear gradient of solvent B was used to optimize purification over a 90 min run. Subsequently, 52 mg of peptide was purified with a final purity of ~98%. The peptide was analyzed by mass spectroscopy, and its mass was determined to be 2310.09 Da (error of <0.0003% from attending mass). Vpr(1−96) was also obtained by automated solid phase synthesis. Wang LL resin (0.4 mmol/g) and amino acids were purchased from Novabiochem. The peptide synthesis was accomplished by using protected amino acids coupled to activation of the carboxyl group of amino acids by HoBt/DCC, leading to 764 mg of crude extract. The resulting mixture was purified by reverse phase HPLC (C4 column, 300 Å, 5 μm, 250 mm $\times$ 10 mm, Ace) using a H_2O/0.05% TFA mixture (solvent A) and acetonitrile (solvent B). A 20 to 80% linear gradient of solvent B over a 90 min run was used to optimize the purification. The final yield was 78 mg at 98% purity of Vpr from a single synthesis experiment. The peptide was analyzed by mass spectroscopy with a corresponding parent peak at *m*/*z* 11394.2.

Circular Dichroism (CD). CD spectra were recorded on a Jobin-Yvon model C8 spectropolarimeter calibrated with *d*-camphor-10-sulfonate. Spectra were recorded at ambient temperature (≈20 °C) in a 0.1 cm path length quartz cell. The peptide concentration in each sample was 40−70 μM, and experiments were performed at pH 3.3 with 30 mM NaCl. Four averaged scans were collected in 0.5 nm interval steps, using an integration time of 2 s and a light bandpass or slit width of 2 nm. Curves were smoothed from 185 to 260 nm using 25 data points, and respective intensities are expressed in mean residue molar ellipticity $[\theta]$, calculated from the equation $[\theta] = 100[\theta]_{obs}/CnL$, where $[\theta]_{obs}$ is the observed ellipticity in millidegrees, L is the optical path length in centimeters (0.1 cm), C is the final concentration of the peptide in molar, and n is number of the amino acid residues.

Differential Scanning Calorimetry (DSC). Lipid films were prepared by dissolving the appropriate amounts of lipid and peptide (at a P:L molar ratio of 1:100) in a mixture of chloroform and methanol (2:1, v/v), followed by solvent evaporation under nitrogen to deposit the mixture as a film on the wall of a test tube. Final traces of solvent were removed in a vacuum chamber attached to a liquid nitrogen trap for 3−4 h. Films were hydrated with 10 mM acetate buffer and 30 mM NaCl (pH 3.5) and vortexed extensively at a temperature above to the main phase transition temperature of the lipid to obtain multilamellar vesicles. The calorimetry was performed on a high-sensitivity differential scanning calorimeter (Calorimetry Sciences Corp.). A scan rate of 0.5 °C/min was used with a delay of 10 min between sequential scans in a series that allows for thermal equilibration. Total lipid concentrations used were 1 mg/mL, providing full hydration of the phospholipid mixtures. Four heating and cooling scans from 0 to 40 °C were conducted to test for reproducibility. Data analysis was performed with the fitting program CPCALC provided by CSC and plotted with Igor (WaveMetrics).

NMR Sample Preparation. The HPLC-purified peptide was dissolved in water at pH 3.5. UV−vis spectra were recorded to quantify the sample, after which additional lyophilization steps were used to prepare a stock solution of peptide. The additional lyophilization steps were necessary to remove the TFA and acetonitrile molecules. Further treatment involved the use of dialysis to remove any impurities that might have been produced during peptide synthesis and remaining after purification. The sample was lyophilized and solubilized or resuspended to a final concentration of 2−4 mM in H_2O at pH 3.3. Peptides for the different preparations, i.e., with and without TFE and DPC, were taken from this preparation. D_2O was used at 5−10% and TFE-d_3 up to 50%; 30 mM NaCl was included in each sample prior to spectral acquisition. A DPC-d_{38} stock was prepared at 500 mM and kept at −20 °C. Unless otherwise mentioned, the pH was always rechecked after any change in the experimental sample conditions, including Vpr titration or DPC addition.

NMR Experiments. Proton NMR experiments were conducted on a Bruker Avance 600 spectrometer operating at a proton frequency of 600.13 MHz. Sets of two-dimensional (2D) experiments (DQF-COSY, TOCSY, and NOESY) were performed under identical conditions (290 K and pH 3.4 ± 0.1 or 5.5 ± 0.1) in H_2O/D_2O solvents as well as in 2,2,2-trifluoroethanol. Typically, 1 mM samples were prepared and NOESY spectra were recorded with a mixing time of 100 ms (to emphasize the shorter dipole−dipole interaction distance of <3 Å) and 200 ms, which includes the long-range direct dipolar interaction (<6 Å) (*21, 22*). All NMR experiments were conducted with 512 equidistant t_1 increment values, to yield 2048 complex data points in the F_2 dimension and 512 real points in the F_1 dimension per FID, and a spectral width of 7600 Hz in both dimensions. The carrier frequency was set to the water resonance. TOCSY spectra were recorded using the MLEV-16 sequence with a total mixing time of 80 ms, acquiring either 64 or 128 scans per t_1 increment. Quadrature detection was performed in the observed dimension, and the time-proportional phase increment (TPPI) method was applied in the indirect one. The NMR data were processed using XWINNMR 3.0 (Bruker BioSpin). All FIDs were zero-filled up to 2K data points to increase the digital resolution before using shifted cosine- and sine-bell window functions in both dimensions. Water suppression was obtained by applying the WATERGATE pulse sequence (*23*), and/or by presaturation of the bulk water magnetization during the recycling delay. Chemical shifts were measured relative to the water signal and residual methanol or TFE signals. Typically, a total of 18 h was necessary for each acquisition experiment, i.e., NOESY, COSY, and TOCSY, though in some cases, the experiment time was doubled to increase the signal-to-noise ratio.

Sequence-specific resonance assignments based on $^1H-^1H$ NOESY cross-peaks form the basis of the structural interpretation of proteins and nucleic acids by NMR spectroscopy, especially when isotopic labeling methods are difficult to implement with proteins that are challenging to express and purify. In this work, all the proton resonance assignments were determined by using well-established 2D NMR methods (*19–22*), broadly described in the literature and based on the following procedure: identification of the individual amino acid residue proton spin systems using DQF-COSY and TOCSY, together with identification of short-, medium-, and long-range interproton distances which manifest nuclear Overhauser effects (NOEs) between se-

quential neighbor residues. NMR samples were usually investigated at pH 3.4 or 5.5, where the glass electrode reading was not corrected for the deuterium isotope effect coming from 10% D_2O.

Structure Calculations. All NMR spectra were processed using Bruker XWINNMR software. NOESY, TOCSY, and COSY spectra were used in SPARKY (*30*) as unique assignment software. The calculated volumes of the NOESY (200 ms) cross-peaks were then exported in XEASY format and used in CCPNMR (*31*) for interatomic distance calibration using the isolated spin pair approximation and the cross-peak between a proton pair of known distance as a reference (Tyr-aromatic and Pro-β protons). The structures were computed from experimental restraints by using the hybrid distance geometry dynamical simulated annealing method (ARIA) (*40*), assigning ambiguous and unambiguous NOEs with ARIA 2.2. Typically, nine iterations using up to 100 structures in final refinements were employed. From the final run, the 10 lowest-energy structures were retained and subsequently used to cross-validate the NOE distance restraints, providing improvements for further calculations (around 40 ARIA runs were employed). Parallel calculations were performed using NIH-XPLOR. The distance restraints were obtained from NOE cross-signal volumes measured on a 200 ms mixing time NOESY spectrum recorded at 290 K by integration of the peaks and conversion into distances by an r^{-6} dependency. A tolerance of 20% was introduced to take integration errors into account. Distances were calibrated using known distances between aromatic protons, and no dihedral torsion angle restraints were included in the calculations. Distance geometry and simulated annealing regularization was performed to embed and optimize initial structures. Of 100 attempts to embed and optimize, the 20 best structures were selected on the basis of criteria of satisfactory covalent geometry, low distance restraint violations, and favorable nonbonded energy and optimized by restrained MD simulations. Distance-restrained MD simulations were carried out in vacuum with a distance-dependent dielectric constant. The dynamics were initiated at 5 K, and the temperature was gradually increased to 1000. The force constants for the distance restraints were set to 2.0 kcal mol^{-1} $Å^{-2}$ during these stages and scaled up to a final value of 30 kcal mol^{-1} $Å^{-2}$ over 6 ps. The system was allowed to evolve for 20 ps at 1000 K, slow-cooled to 300 K in 14 ps, and equilibrated for 10 ps. The coordinates were saved every 0.5 ps; data from the last 4 ps were averaged, and the resulting structures were subjected to conjugate gradient minimization until a final gradient of 0.1 kcal mol^{-1} $Å^{-2}$ was reached. All dynamics were carried out with a time step of 1 fs. These 10 last structures were used for structure evaluation using PROCHECK (*32*). The statistical results are summarized in Table 1 of the Supporting Information.

MD Simulations. CHARMM (*34*) was used for system construction, simulation, and analysis, employing the CHARMM lipid force field, including recent refinements for saturated chains (*41*). The experimentally determined structure of the peptide was used as the starting configuration, while the DPC molecules were built from idealized geometries. The peptide structure was investigated in two systems. The first system consisted of one peptide, 100 DPC molecules, and 6370 water molecules with the peptide initially centered in the micelle. A second simulation, for exploring the peptide structure in an aqueous environment, consisted of the peptide and 2783 water molecules. In both simulations, amino acids Lys and Arg had a charge of +1, amino acids Asp and Glu had a charge of −1, and all other amino acids were uncharged, resulting in a total charge of the peptide of −1. To account for the experimental salt concentration and to make the system neutral overall, four sodium and three chloride ions were added to the micelle simulation and two sodium ions and one chloride ion to the water simulation. All simulations were carried out with constant normal pressure (1 atm) and constant temperature (20 °C), using extended system algorithms (*35*). Both systems were equilibrated by restraining the complete peptide structure at first and then subsequently releasing the amino acid side chains and finally the entire peptide. The micelle simulation was carried out for 60 ns, while the water simulation was carried out for 80 ns, using a 2 fs time step. Electrostatic forces were computed with the smooth particle mesh Ewald algorithm; bonds involving hydrogen atoms were constrained by means of the SHAKE algorithm, and conformations were saved once per picosecond for subsequent analysis (*25*). Average structures of the peptide were calculated using the last 10 and 15 ns of the trajectory for the micelle and water simulations, respectively.

RESULTS AND DISCUSSION

Viral proteins such as Gag p6 and many others found across all life kingdoms are often termed intrinsically unstructured proteins (*27*), or natively unfolded, which means that such proteins act as a collection of highly dynamic species where torsion angles have a much broader dispersion compared with the Ramachandran preferred regions (*26*). Such proteins present a great challenge to experimental study due to biophysical properties that depend on certain conditions being met such as the availability of the correct partner(s), the correct cellular compartment, the presence of specific osmolites, and even oxidative conditions. Therefore, a common practice for avoiding these problems is to make preparations in organic solvents, often overused in biological structural studies because of their tendency to stabilize specific secondary motifs, such as α-helices in the presence of 2,2,2-trifluoroethanol. A drawback is that such structurally biased results may provide information about an ensemble of structures that differ from those inside a cell. In some proteins, the effect of TFE may be negligible, but the fact that TFE molecules preferentially aggregate around hydrophobic amino acids making a coating that displaces water molecules and removes alternative hydrogen bonding partners (*43*) should be considered, especially when the study intends to probe protein−protein interactions. The 2D NMR spectra of p6ct in water recorded in this study show patterns characteristic of those found in unfolded peptides; i.e., the dispersion of resonances is much narrower compared with those of both the TFE and DPC studies, and medium-range NOEs, e.g., $d_{\alpha N}(i, i + 2; i, i + 3)$, and $d_{\alpha\beta}(i, i + 3)$ connectivities, are scarce or absent (*37*). DPC also provides a medium that accommodates peptides with amphiphilic characteristics, while still providing a water-based solvent, enabling a dielectric constant of ∼80 in water (≅4 inside the micelle) at 20 °C, which would not be possible in TFE. The DPC system avoids the use of organic solvents, which

modify not only the dielectric constant but also the hydrogen bond acceptor/donor behavior that gives water its unique solvent properties. In addition, DPC micelles may to some extent mimic biological membranes which are present during the interaction between p6 and Vpr or other partners. Taking into account the fact that both p6ct and Vpr may modify each other's 3D structure by discretely reshaping the folding pathway otherwise not available, we find it is imperative that the 3D structures of both p6ct and Vpr should be determined as part of the complex. This is a daunting task given that both peptides are difficult to produce using traditional methods of isotopic labeling. The reshaping of the folding pathway is a peculiar feature in proteins, where Vpr may be a good example. A recently proposed model points out that a unique cis−trans isomerization in P35 may change the overall folding of Vpr, with consequences at the level of encapsidation and even replication (*45*). Such important structural rearrangements were never reported before when the studies included only small portions of Vpr (*46, 47, 52*) that a priori excluded that region containing the pivoting P35. The fact that a particular proline isomeric state may govern such an event emphasizes the plasticity that some viral proteins may adopt in different phases of infection. Such examples illustrate how the multiplication of tasks and partners can be achieved by a single peptide, simply by having a flexible and dynamical folding landscape and adapting it according to its localization or the molecular partners that are available. The lack of rigid global folding and the fact that the protein is sampling multiple conformations mean that the contact surfaces can be readily modified without requiring a high-energy process. Such structural plasticity provides multitasking properties for some proteins, an important feature for the success of the virus, especially taking into consideration the fact that the virus packs a short genome (*42*), which usually produces just a few proteins, and many obstacles need to be bypassed during the HIV infection process. Figure 1 depicts the CD spectra of p6ct in different solvents (water, water/TFE mixtures, and DPC micellar suspension). As seen in Figure 1, the spectrum of p6ct in water (red) presents a negative band around 200 nm and no positive bands. This indicates that the p6ct peptide is unstructured in water, as reported previously (*51*), but becomes structured in the presence of TFE (black) and in a membrane-mimicking agent such as DPC, red-shifting the main negative band from ~200 to 208 nm (parallel $\pi \rightarrow \pi^*$ transitions) with a positive 190 nm band (perpendicular $\pi \rightarrow \pi^*$ transitions), indicating formation of helix. The addition of TFE gradually increased the ellipticity, and no significant alterations in the helical amount were observed above 50% TFE content. In DPC, the ellipticity increased to a molar ratio of 1:100, well above the minimum micelle size (~50 detergent molecules) and 100 times above the critical micellar concentration (1 mM).

Probing p6ct and Membrane Interaction Using DSC. Differential scanning calorimetry has been used to probe the properties of the interaction between p6ct and DPC micelles, which share some chemical properties with DMPC lipids (both are zwitterionic and have choline heads). DMPC vesicles without peptide exhibit two very well characterized endothermic events. The first (pretransition) originates from the conversion of the lamellar gel phase $L_{\beta'}$ to the rippled gel phase $P_{\beta'}$ around 8.3 °C, which is characterized as being less energetic and less cooperative (Figure 2). The second much sharper (main) transition due to the conversion of the rippled gel phase to the lamellar liquid-crystalline phase L_α is highly energetic and centered around 22.8 °C. Those values closely resemble previous reports in the literature for the DMPC system (*28, 29*). The thermogram in Figure 2 reveals two important aspects regarding the peptide distribution in a DMPC model membrane. The data show that the peptide interacts at the headgroup level since the pretransition phase completely vanishes (expansion panel), indicating a strong effect on headgroup tilt. The head-to-head average distance

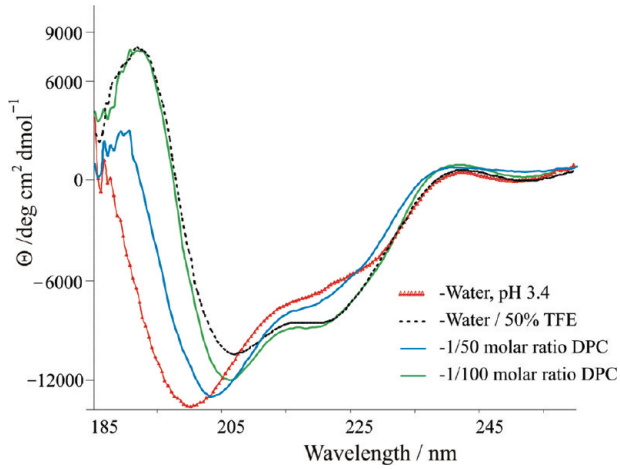

FIGURE 1: Circular dichroism spectra of p6ct. The spectrum of p6ct in water (red) presents the typical random coil negative broadband around 200 nm and no positive bands. The pattern depicted indicates that p6ct is unstructured in water or has just residual secondary motifs. In the presence of organic solvents, p6ct tends to adopt an α-helix structure, as in the case of TFE (black) but also in the presence of membrane-mimicking agents such as DPC, red-shifting the main negative band from ~200 to 208 nm with a positive 190 nm band, indicating formation of helix. The addition of TFE gradually increased the ellipticity, and no further significant alterations in the helical content were observed above 50% TFE. In DPC, the ellipticity increased to a molar ratio of 100 (green), well above the minimum micelle size (~50 detergent molecules) and 100 times above the critical micellelar concentration (1 mM). All preparations were buffered with citrate at pH ≈3.4 containing 30 mM NaCl.

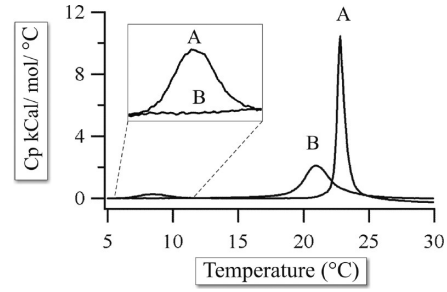

FIGURE 2: DMPC vesicle thermogram without peptide (A) that exhibits two very well characterized endothermic events. The first (pretransition) originated from the conversion of the lamellar gel phase $L_{\beta'}$ to the rippled gel phase $P_{\beta'}$ around 8.3 °C. The second much sharper transition (main peak) due to the conversion of the rippled gel phase to the lamellar liquid-crystalline phase L_α is centered around 22.8 °C. Thermogram B was recorded for DMPC in presence of p6ct (at a P:L molar ratio of 1:100), in 10 mM acetate buffer and 30 mM NaCl (pH 3.4). Total lipid concentrations used were about 1 mg/mL, resulting in full hydration of the phospholipid mixtures. The scan rate used was 0.5 °C/min with a delay of 10 min between sequential scans in a series that allows for thermal equilibration.

increased due to the insertion of the peptide at the surface level, thereby modifying ΔH, a behavior commonly seen in membrane-adsorbed peptides (*29*). A second important observation is that the peptide intercalates between the lipid fatty acid chains, however not strongly, since only a modest (30%) decrease in the enthalpy and entropy of the main transition is observed due to a disruption of the fatty acid chain van der Waals interactions. Finally, a decrease in the T_m is observed (~2 °C), indicating that the peptide favors the L_α phase. This means that the peptide interacts more favorably with the fluid lipid phase, because its partial interaction with the fatty acid chains leads to a decrease in the cooperativity of the main phase transition ($\Delta T_{1/2}$). There is no split in the main phase transition, or appearance of shoulders, indicating that the peptide is evenly distributed in the lipid surface. When the roughly 40−50% α-helix content of p6ct in DPC micelles is taken into consideration, calculated from CD spectral analysis and MD simulations, an α-helix adsorbed into the micelle with the hydrophobic portion of the helix protruding through the micelle aliphatic core, leaving its highly flexible terminal regions in contact with the solvent and head groups of DPC, was anticipated. Samples containing the peptide alone exhibited no thermal transitions over the temperature range employed. This indicates that over this temperature range the endothermic events observed in this study arise solely from phase transitions of the phospholipid vesicles and not from peptide denaturation.

NMR Studies in TFE, and DPC and Sequential Assignment of p6ct. The assignment was accomplished by employing a combination of NMR experiments conducted at different pH values and solvents (TFE and water) to follow chemical shift pattern displacements within the same spin system. This simple method often allows deconvolution of overlapped peaks and a better assignment of resonances. Initially, a 2D ^{1}H NOESY NMR experiment was used to characterize the regions with strong $d_{NN}(i, i + 1)$ and $d_{\alpha N}(i, i + 1)$ connectivities, together with the spin system characterization from the homonuclear Hartmann−Hahn spectroscopy (HOHAHA/TOCSY) (*24*) to delineate intraresidue connectivities via two- and three-bond H−H *J* couplings, always confirming the symmetry of those assigned peaks. Using an iterative assignment procedure, it is possible to obtain a large number of intra- and inter-residue connectivities, including side chain methyl groups, and to assign nearly the complete sequence using almost all NOEs present in the spectrum (*23*). This resulted in sequential assignments concerning primarily residues with strong $d_{NN}(i, i + 1)$ and medium-range $d_{\alpha N}(i, i + 2; i, i + 3; i, i + 4)$ NOEs (*23*), commonly associated with α-helices. This is consistent with an α-helix (L35−G46) flanked by two unstructured terminal regions (residues 32−34 and 47−52). Both solvents gave sufficiently well-resolved spectra for assignment of almost all resonances but not for the accurate measurement of the *J* coupling constants.

In Figure 3, NOESY spectra (τ_m = 200 ms) of p6ct in 100 mM DPC (pH 3.4) containing 30 mM NaCl are shown presenting the key NOE connectivities used for the assignment procedure. The NH−Hα sequential connections are colored dark green. Due to a wide distribution of the side chain protons in the spectrum, all NOEs from the NH−Nα region were unambiguously successfully assigned. This analysis provided the basis for sequence-specific resonance assignments of the polypeptide segment from D32 to Q52. In all NMR spectra, suppression of the water signal was achieved with WATERGATE or/and with a water presaturation. Residual methanol or perdeuterated TFE signals were used to calibrate the spectra and kept as a reference for the titration experiments. To resolve ambiguities in NMR spectra due to overlapping peaks, several acquisitions at different temperatures and pHs were performed to follow coherently shifting groups of peaks. In panel a, the methyl region of the side chain proton spectral region is shown, and in panel b, the NH−Hα region is shown. A superposition of two different spectra illustrates the nature of a major challenge in structural biology, i.e., the solvent choice. The blue contours depict p6ct NOESY spectra in ≈50% TFE, while red contours depict p6ct in 100 mM DPC, each at pH ≈3.4. The major differences are remarkably accentuated in some amino acids, such as K33, Y36, L44, and D48. In the DPC spectrum, the chemical shift dispersion is vastly augmented in both dimensions, which greatly facilitates the assignments. Both P37 and P49 are in the trans conformation, readily deduced from the strong $X_{(i-1)}$−P correlations in the αH−δH region of the NOESY spectrum. No evidence of $X_{(i-1)}$−P αH−αH correlations (indicative of cis isomers) was found. It is apparent that some NOE connectivities, mainly in the NH−Hα region, are similar both in TFE and in DPC micelles, even though the chemical shift distribution diverges significantly when both solvents are compared. This indicates that the peptide has comparable secondary structures in TFE and DPC environments but that the dynamics, i.e., the multiconformation sampling, seems reduced in DPC where we can observe more inter-residue connectivities, an effect most visible between side chains. The importance of the solvent is further apparent when we examine titration experiments involving Vpr. The data concerning the NH−Hα connectivity peaks suggest that in both solvents (TFE and DPC) an α-helical segment is formed at 293 K.

Often the collection of backbone and side chain NOE assignments is sufficient to define the 3D structure of proteins with precision and accuracy comparable to those obtained by X-ray crystallography (2 Å) (*33*). However, to further improve the quality of the structure of p6ct and to improve our understanding of the ensemble distribution, we refined the structural model by MD simulations in the presence of DPC and in water alone. This is particularly important because it further improves the structure quality of the peptide in the presence of the experimental solvent, e.g., DPC, and NaCl, which unfortunately is not possible in the common annealing protocol when using Aria or NIH-Xplor packages alone. In Figure 4, we present a comparison between the 10 lowest-energy structures calculated by NMR (panel a) and the seven final structures (sampled every 2 ns) from a 60 ns MD run. The MD simulation was started with the peptide in the averaged NMR structure calculated using XPLOR. Notably, it becomes apparent that the helical domain is longer in the MD simulation when compared to the NMR- XPLOR calculation ensemble. This may be because calculations in both Xplor and in Aria do not accommodate a complex solvent such as DPC micelles, or the presence of salts, which seems to be important in stabilizing the C- and N-termini of p6ct. This is further evident if we look to the Na^+ ion positioning at the ends of the helices, especially D32 which

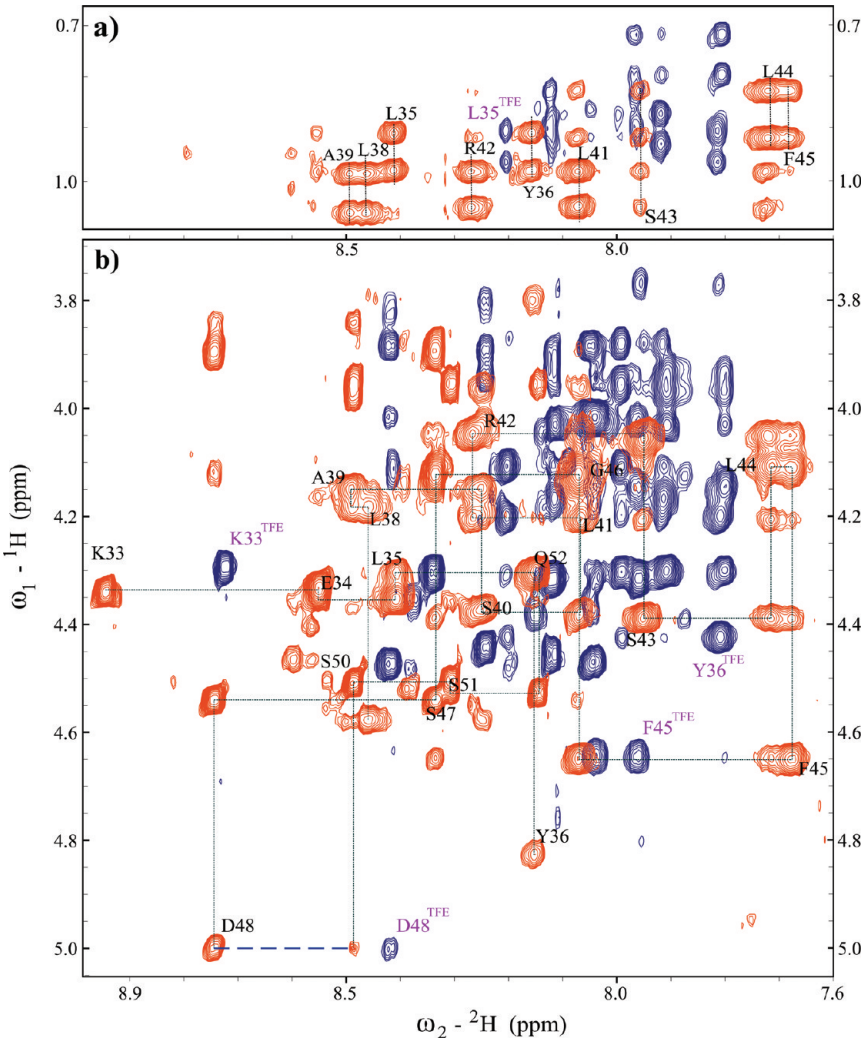

FIGURE 3: Presentation of two NOESY (T_m = 200 ms) spectral regions. In panel a, the side chain proton region is shown, and in panel b, the NH−Hα region is shown. Blue depicts the NOEs attributed to the p6ct sample in 50% TFE (pH 3.4) superposed on the p6ct sample (red) in 100 mM DPC-d_{38} at the same pH (both samples contain 30 mM NaCl). The major differences are remarkably accentuated in some specific amino acids, such as K33, L35, Y36, F45, and D48 (purple labels). The sequential NOEs connectivities [$d_{\alpha N}(i, i + 1)$] are outlined in dark green. The blue dashed line represents a $d_{\alpha N}(i, i + 2)$ connectivity conjoining D48 and S50 (both amino acids flanking P49).

forms a salt bridge for approximately the last 40 ns of the run, helping to stabilize the helix. At the C-terminus, sometimes a Na^+ ion is present as well but not resident for such long periods. We also performed a second simulation starting with the same peptide structure but using only water as the solvent (results not shown). It is interesting to note that in the water run (≈80 ns) the salt ions are never resident (salt bridging) to any amino acid and the peptide secondary motif resembles more the original from the NMR experiments. In the DPC system, the helix content expands from the LASLRSLF[45] domain obtained by NMR to the KELYPLASLRSL[44] domain during the MD simulation (±1 amino acid on each end depending on which structure is chosen from the final ensembles). The helical motif spans without a curvature or bend a micelle comprising 100 DPC molecules having an approximate diameter of 50−60 Å. The NMR structures populate around 58% of the torsion angles in Ramachandran favored regions, while the MD ensemble conformers for the last 10 ns show well-defined α-helical motifs, with 95% of the torsion angles populated in Ramachandran favored regions (values calculated using MOLPROBITY from http://kinemage.biochem.duke.edu/molprobity/).

The larger extent of the α-helix could also be an artifact due to the initial location of the peptide in the center of the micelle. The equilibrium location of the peptide appears to be on the surface of the micelles (vide infra); however, the initial very hydrophobic environment could have induced the formation of the longer α-helix, where unstructured and thus not hydrogen bonded motifs of peptides and proteins are very unfavorable.

Interaction of p6ct with Vpr. To study the interaction between p6 and Vpr, we decided to use full-length Vpr as opposed to the proteins used in other studies (*36*), since we cannot exclude a structural rearrangement such as a clamp effect from the Vpr three helical motifs upon p6ct binding. Interestingly, recent results demonstrating an interaction between Alix and a late $LYPx_nLxxL$ domain (*44*) provide evidence for the Tyr side chain intercalation between two Alix α-helices. Another recent study proposed the possibility of a similar mechanism, based on a pivoting proline (P35) on Vpr (*45*). Thus, it seems appropriate to study the interaction between these two proteins using the full-length Vpr protein, and if possible having the entire p6 as well. Truncating Vpr may lead to alternative unrealistic binding

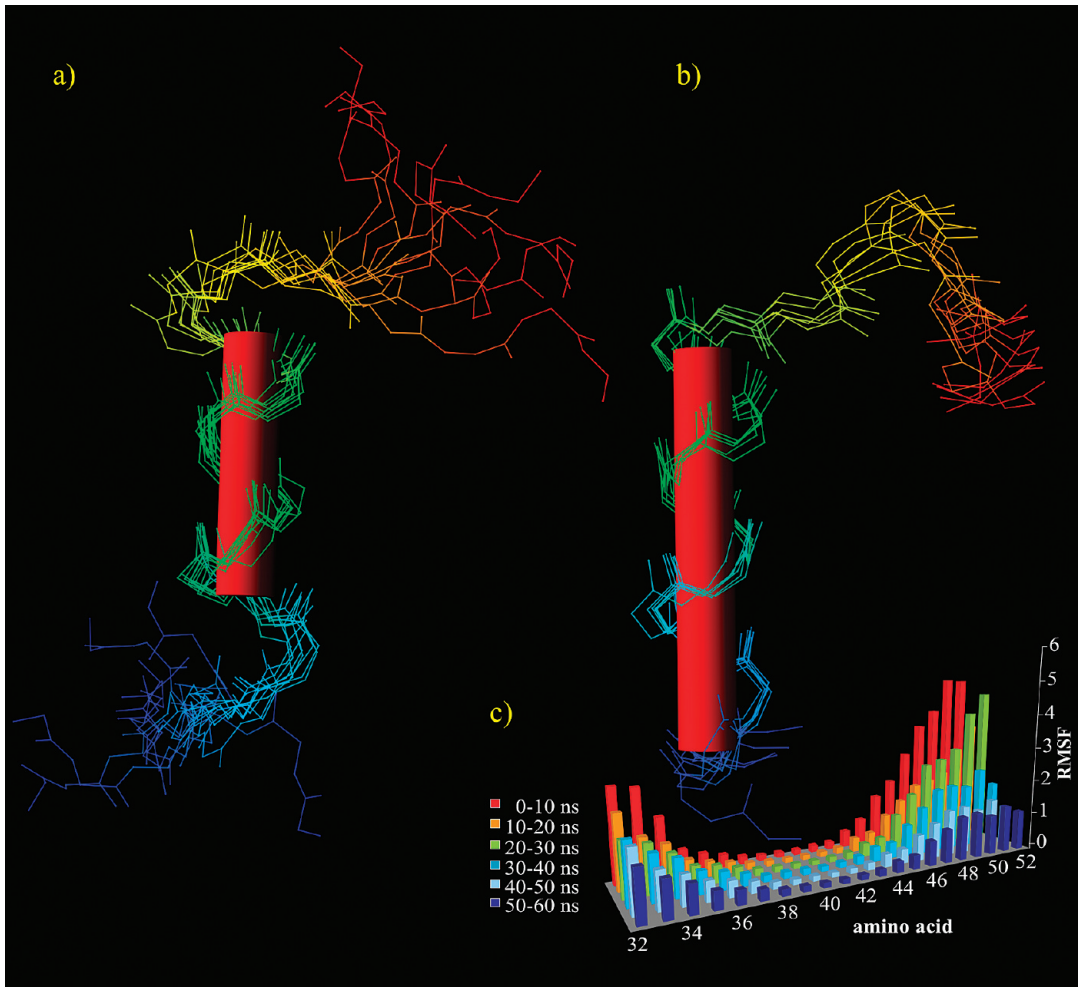

FIGURE 4: Overlay of the 10 energetically most favored structures calculated using NIH-XPLOR (a). Initial restraints were obtained in 100 mM DPC (pH ≈3.4) and 30 mM NaCl; volumes were calculated in Sparky, and conversions to distance restraints were set in CCPNMR. The system was allowed to evolve for 20.0 ps at 1000 K, slow-cooled to 300 K in 14.0 ps, and equilibrated for 10.0 ps. All dynamics were carried out with a time step of 1.0 fs. In the ensemble in panel b, the final 10 structures from the last 10 ns, extracted from a 60 ns MD run using the CHARMM force field with a time step of 2 fs (blue depicts the N-terminus), are depicted. Panel c shows the root-mean-square fluctuations of all residues in periods of 10 ns.

properties, which together with hydrophobic force suppressor solvents such as TFE could mislead the interpretation of the binding model and properties. Although we cannot exclude the possibility that the p6 N-terminal domain is important for Vpr binding, the literature provides numerous studies reporting that Vpr binds p6 in a C-terminal domain (vide supra). The use of amphiphiles in water solvent together with the titration of p6ct to full-length Vpr (10:1; 5:1; 2:1, and 1:1 molar ratios) allowed us to determine the amino acids in p6ct and which chemical shift values deviated most from free p6ct NMR experiments. Figure 5 shows an example of such a procedure, where for the sake of simplicity only the 5:1 (p6ct:Vpr) molar ratio is shown. The red contours represent the NOESY spectra at 293 K of free p6ct. The addition of Vpr into the solution readily modifies some NOE peaks, especially E34, L35, and Y36, which can be appreciated in blue overlaid spectra. Additionally, the almost complete disappearance of the NOEs due to the interaction between δ protons (HD) from P37 and the Y36 NH proton can be seen in these spectra. This reveals a dramatic change in this spectral region where similar contours are explicit for other protons in the respective spin systems mentioned before. There is also a progressive disappearance of the $d_{\alpha N}(i, i + 2)$ connectivity from G46 and D48 around 8.74 and 4.12 ppm. Several new peaks from Vpr titration appear in the spectra, with special emphasis to the regions around 8.95 ppm (horizontal) and 4.3 ppm (vertical), and as well the region from 8.3 to 8.7 ppm (horizontal) and around 4.7 ppm (vertical), which were positively identified as Vpr. The chemical shift differences registered during p6ct titration with Vpr are summarized in Figure 6, which displays the NH protons, α-protons, and β-protons in panel a, for a molar ratio of p6ct to Vpr of 5:1, and the NH proton titration pattern for molar ratios (p6ct:Vpr) of approximately 10:1 (green), 5:1 (red), and 2:1 (blue) in panel b. The interaction between p6ct and Vpr was also probed by plasmon waveguide resonance (PWR), and a considerably higher affinity was found for the interaction of Vpr with an egg PC bilayer in the presence of p6ct ($K_D = 0.8$ μM) than in the absence of p6ct ($K_D = 70$ μM). Detailed information about this experiment is provided in the Supporting Information and summarized in Figure S1.

MD Simulations of p6ct in DPC Micelles. Molecular dynamics studies proved to be a valuable tool for understanding the partitioning of the peptide into the micelle, providing snapshots of the dynamics and structure of the p6ct−DPC complex. These results can be better seen in Figure 7, where the final snapshot of a 60 ns DPC micelle

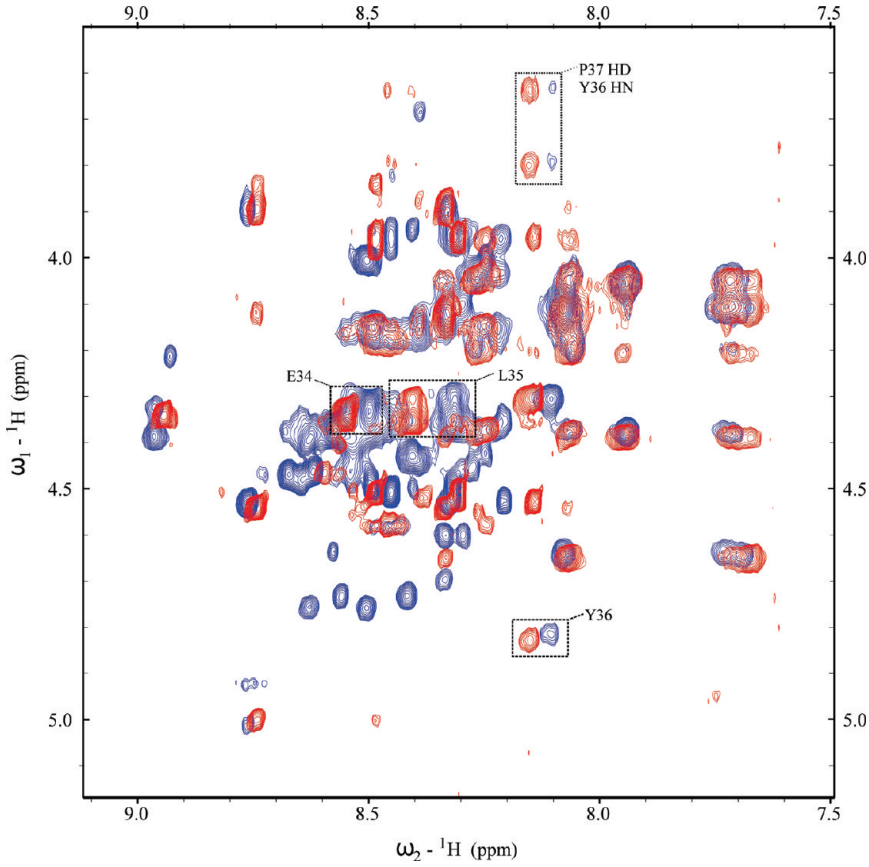

FIGURE 5: NOESY (T_m = 200 ms) contour plot showing the NH−Hα region of p6ct in 100 mM DPC-d_{38} (pH 3.4) with 30 mM NaCl (red). The contours of the titration of Vpr into the same p6ct sample are colored blue. The blue spectrum was obtained at a molar ratio of p6ct to Vpr of 5:1. Dotted boxes represent the three amino acids with the most significant chemical shift displacement (E34, L35, and Y36).

simulation (water molecules omitted) is shown. The peptides on the surface correspond to the six final structures collected at the end of the run (to simplify the figure, we depict only the last micelle structure). During the setup of the MD simulation, the peptide was placed in the center of the micelle. However, from the beginning of the simulation, the peptide continually moved to the interface of the micelle. After simulation for 12 ns, the peptide reached the interface and one side of the helix became exposed to the surrounding water. After 17 ns, one side of the peptide is totally accessible to surrounding water molecules while the other side is facing the DPC molecules. This orientation of the peptide remains stable for the remaining 43 ns of the simulation, and the α-helix is incorporated into the surface of the micelle between the choline headgroups. In the peptide structures, the hydrophobic amino acids are colored orange (L35, L38, A39, L41, L44, and F45), showing that the α-helix is in an optimized conformation and an orientation in which those residues establish contacts with the hydrophobic portion of DPC, i.e., the aliphatic chains. In contrast to the XPLOR structure, P34 is also embedded within the hydrophobic moiety of the micelle, and that seems to be an important factor stabilizing the extended α-helix found in the MD simulation. The peptide is inserted into the micelle surface in a favorable conformation, maximizing its amphipathic properties shown in panels b and c of Figure 7. Interestingly, p6ct does not adapt itself to the micelle positive curvature as is often observed in structural studies with peptides codissolved in micellar systems. With the exception of L35 and Y36, all the remaining hydrophobic residues stretch over the peptide surface that is in direct contact with the micelle hydrophobic core. Overall, p6ct seems to be embedded between the micelle headgroups.

After simulation for 21 ns, a sodium ion (Figure 7, shown as yellow spheres) binds to the N-terminus via residues D32 and E34 and remains there until the end of the simulation. Both D32 and E34 are involved in salt bridges with the Na^+ ion. At the C-terminus, another Na^+ ion forms a salt bridge with D48, but during the run, this Na^+ ion is less strongly bound than the one found at the N-terminus. Both Y36 and E34, which represent the two amino acids with a larger chemical shift difference when titrated against Vpr, have their side chains pointing outward (ball and stick) to the solvent, and L35 (which tops the relative intensity scale) is partially exposed (Figure 7a). At the C-terminal end of p6ct, Q52 also exhibits significant chemical shift differences together with S50 but not S51. An interesting observation is that although S43 seems more exposed to the water solvent than S40, the latter presents a level of relative intensity in chemical shift deviation comparable to that of S50. S40 is also in the same surface side of the helix in a relative orientation comparable to that of Y36, and their chemical shift deviation upon titration with Vpr (5:1 molar ratio) is somewhat important (approximately −0.035 ppm); thus, it may be indicative that S40 also participates directly in the interaction with Vpr. The entire C-terminal region, which is more hydrophilic, seems to make extended contacts with the solvent, protruding less into the micelle surface. In general, the highly dynamic nature of the micelle accommodates rotation fluctuations along the α-helix stretch, orienting the

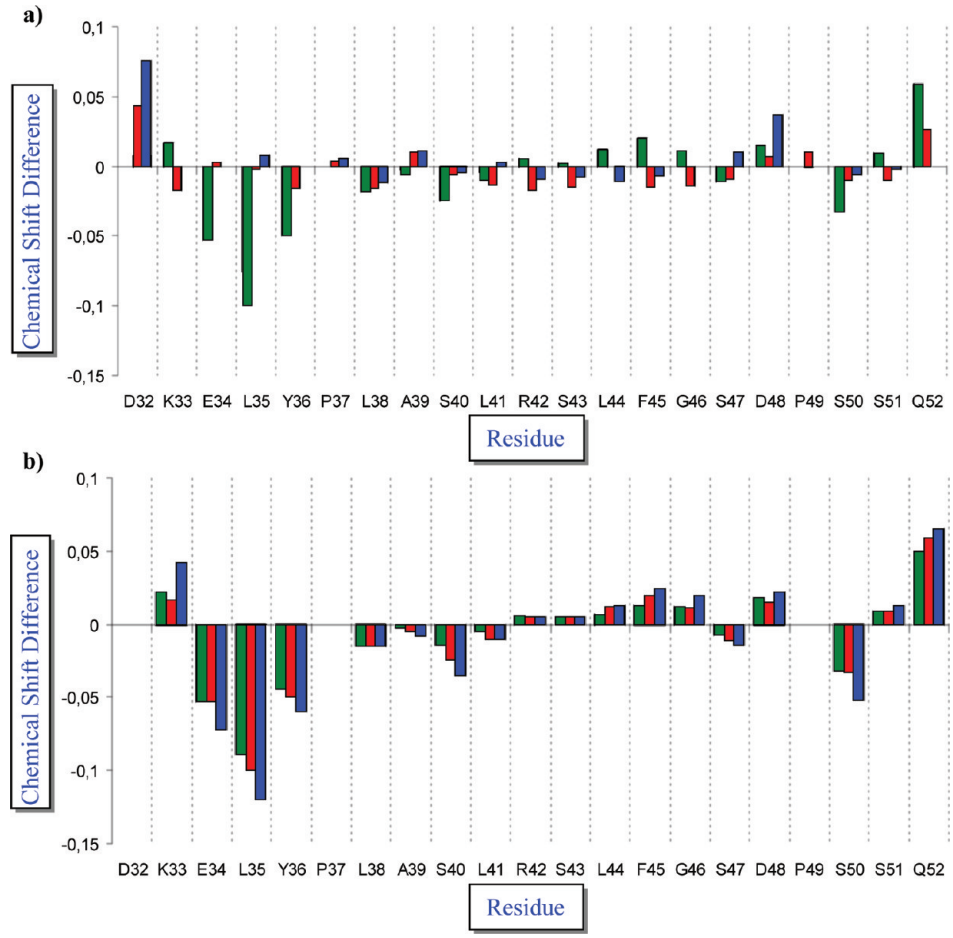

FIGURE 6: Chemical shift difference (parts per million) analysis from p6ct titration to full-length Vpr. In panel a, NH protons (green), α-protons (red), and β-protons (blue) are shown for a molar ratio of p6ct to Vpr of 5:1. In panel b, the NH proton titration pattern for molar ratios (p6ct:Vpr) of 10:1 (green), 5:1 (red), and 2:1 (blue) are shown. Values below 0.01 ppm should be read with care.

above-mentioned amino acids and exposing them more or less to the solvent. In the bottom part of Figure 7, the hydrophobic residues are marked with purple dashed lines and are more visible in the cut shown from the C-terminus in panel b, and in an ≈70° tilt in panel c. Keeping in mind that the peptide did not reach equilibrium inside the micelle but rather on the surface, as supported by the DSC data, and as well PWR, we can infer some possible similarities with biological membranes. For example, Gag p6 could be adsorbed on the surface of a cellular membrane directly or indirectly, helping the budding mechanism while interacting with proteins from the endosomal sorting complex (ESCRT-1), a hypothesis that should be further explored.

CONCLUSION

The results presented here provide new detailed molecular information necessary for continuing to decipher the complex proteomic interactions, especially posed by HIV-1 proteins during the sorting of virions from infected cells. We found evidence that Y36, a highly conserved residue from Gag p6, together with E34 and L35 plays a major role in the interaction with Vpr, but not likely being the sole junction point between the two peptides. The hydroxyl group from Y36 seems to drive the positioning of the side chain in an orientation exposed to the solvent. The amphipathic α-helix, a common motif in membrane binding peptides and proteins, forms in response to both types of environments present in micellar systems, e.g., hydrophobic and hydrophilic. Such an environment is also present in both Gag p6 and Vpr during the process of cell infection by HIV-1. Previous results obtained for the interaction of p6 with Vpr did not provide such an environment but rather employed a mix of water and organic solvents where the average dipole moment and ionic properties are vastly different. Such differences may be the reason for the 5-fold increase in chemical shift displacements and for the different amino acids involved in Vpr binding reported in this study. Whereas P37 seems to be the α-helix breaker in the NMR structure, in the case concerning the ensemble of structures obtained by MD, probably due to the presence of a hydrophobic environment provided by the DPC molecules, they seem to be part of an extended α-helix. In addition, the importance of the ELYP[37] sequence demonstrated in this work may explain why previous results with both sequences Gag p6(38−52) and p6(37−46) were unable to incorporate Vpr (*38*). Moreover, the ELYP[37] sequence resembles the YP*X*L sequence previously described as being crucial for interaction with Alix (*39*), where again Y36 seems to be the key amino acid. We also should take into consideration a dual binding mode or sequential mode between p6 and Vpr and/or Alix. The dissociation constants determined before for a short p6 peptide (p6−16) and Alix (*39*) showed a complex curve that required fitting with a two-site model, whereas the fitting for p6ct with Vpr in an egg PC membrane yielded a single-

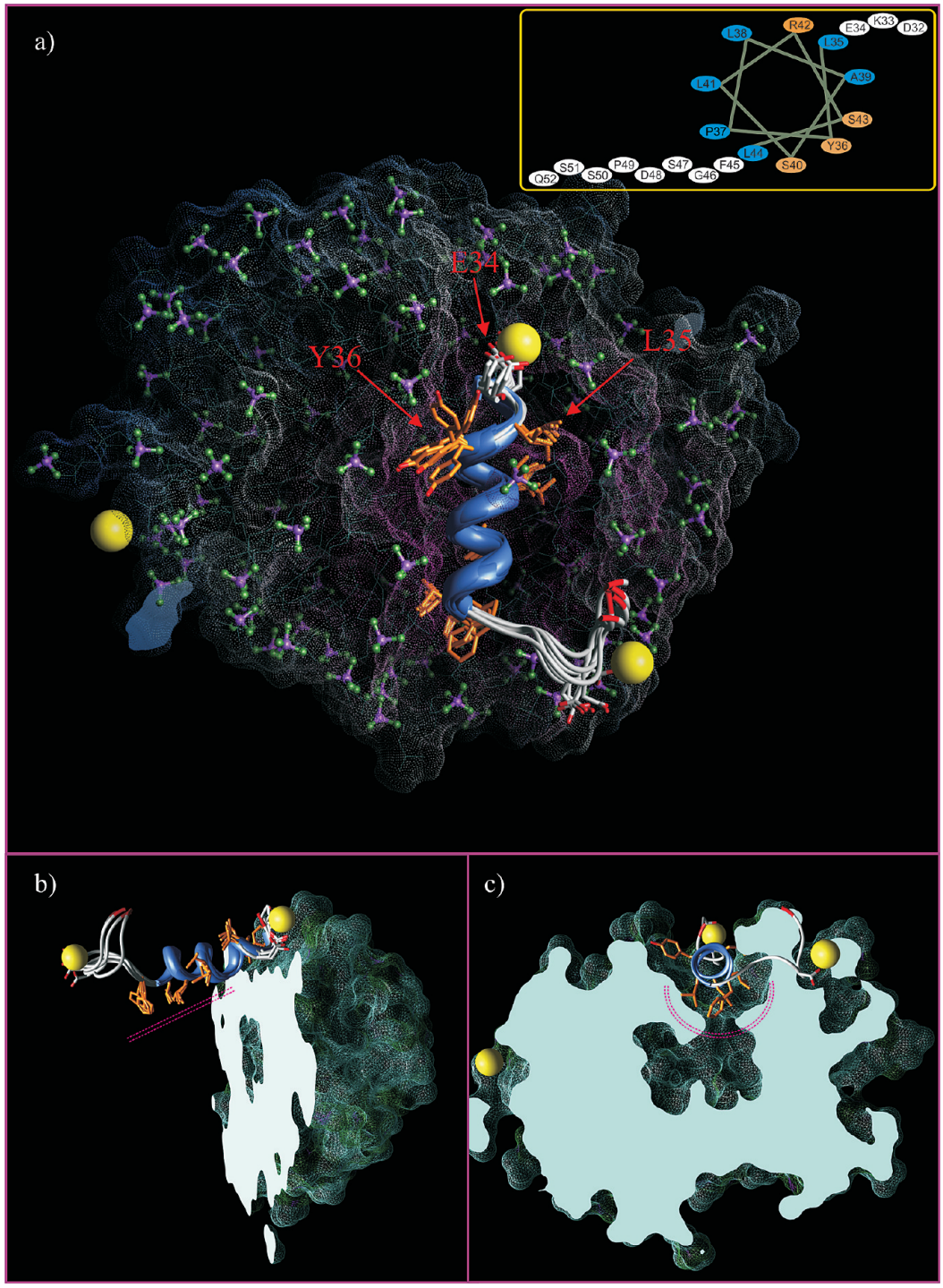

FIGURE 7: (a) Last six p6ct structures from the 60 ns MD simulation in a DPC micelle with 30 mM Na^+ (yellow spheres). In the top right corner inset is depicted the p6ct sequence in a wheel-pattern projection with hydrophobic residues colored blue and hydrophilic residues orange. The DPC choline headgroups are represented in a ball-and-stick model (green and purple). The amino acids which display the larger chemical shift differences in the presence of Vpr, e.g., E34, L35, and Y36, are exposed to the solvent and therefore easily accessible to any interacting partner. A patch of hydrophobic amino acids (pink double-dashed lines) comprising L38, L41, L44, and F45 is totally embedded in the DPC hydrophobic moiety. To emphasize this point, panels b and c show the same snapshot with cuts through the micelle from the side and C-terminus of the peptide, respectively.

site binding. It is our perception that we need much more complete experiments with these four "partners" before any models can be approximately drawn.

We also present novel results concerning a possible interaction between Gag p6ct and cellular membranes. In the literature, only the N-terminal portion of Gag matrix (MA), which is naturally myristylated (*48, 49*), is considered responsible for the interaction with biological membranes. The amphipathic α-helix presented here, as obtained by NMR or derived from MD simulations, is not long enough to fully span a normal bilayer. However, the short amphipathic domain may be long enough to drive the stable partition and deposition of Gag p6 peptides to the surface of biological membranes. This would significantly increase the local concentration of the peptide since the stochastic distribution would be reduced from three to two dimensions, increasing

the chance of encounter between species during the sorting mechanism. Although it is not known yet, HIV-1 Gag translation can possibly occur near the plasma membrane (*50*), facilitating its adsorption into membranes and working as a docking bay for other proteins to meet or directly interact, such as proteins from the endosomal sorting complex assisting in the process of virion formation. The lack of supporting data in the literature concerning this new hypothesis should not exclude a possible more direct interaction between Gag p6 and the cellular membrane or sorting vesicles. This is a possibility that deserves further exploration using both in vitro and in vivo experiments, especially after some results (*36, 51*) and current work have shown that p6 does not fold in a stable secondary structure in water base solutions, as opposed to the situation in which a membrane-mimic environment is present.

Crucial experiments need to address the incorporation of isotopically enriched amino acids in stretches of Gag p6 identified in this study as being new in binding to Vpr, e.g., E34−P37, and as well in some key residues in Vpr reported in other studies (*45*), such as the region surrounding P35. Specifically labeled samples for studying not only the structure but also the dynamics of the event would be a remarkably valuable tool for probing at the molecular level Gag p6 and Vpr interactions, especially if some sort of clamp mechanism is present involving large amplitude motions in any motifs of the three helical domains of Vpr. It is important to continue to evaluate this region of HIV-1 Gag, which is associated with important mutations such as the Y36S and L41P mutations, which render the virus incapable of infection, or the Y36F mutation, which makes the virus 300-fold as infectious as the wild type (*9*). With detailed molecular information, new avenues regarding the discovery of original therapeutic targets for disrupting virus−cell interactions (*50*) can potentially be explored, such as those occurring during the assembly and sorting processes of HIV-1 virions.

SUPPORTING INFORMATION AVAILABLE

Plasmon waveguide resonance used to determine the dissociation constants for Vpr in the presence and absence of incorporated p6ct in an egg PC planar lipid bilayer (Figure S1, panels A and B, respectively) and NMR structural statistics for the 20 structures of the p6ct(32−52) domain (Table S1). This material is available free of charge via the Internet at http://pubs.acs.org.

REFERENCES

1. Gottlinger, H. G., Dorfman, T., Sodroski, J. G., and Haseltine, W. A. (1991) Effect of mutations affecting the p6 gag protein on human immunodeficiency virus particle release. *Proc. Natl. Acad. Sci. U.S.A. 88*, 3195–3199.
2. Huang, M., Orenstein, J. M., Martin, M. A., and Freed, E. O. (1995) p6Gag is required for particle production from full-length human immunodeficiency virus type 1 molecular clones expressing protease. *J. Virol. 69*, 6810–6818.
3. Freed, E. O. (2002) Viral late domains. *J. Virol. 76*, 4679–4687.
4. Wilkinson, T. A., Tellinghuisen, T. L., Kuhn, R. J., and Post, C. B. (2005) Association of sindbis virus capsid protein with phospholipid membranes and the E2 glycoprotein: Implications for alphavirus assembly. *Biochemistry 44*, 2800–2810.
5. Usami, Y., Popov, S., and Göttlinger, H. G. (2007) Potent rescue of human immunodeficiency virus type 1 late domain mutants by ALIX/AIP1 depends on its CHMP4 binding site. *J. Virol. 81*, 6614–6622.
6. Martin-Serrano, J., and Bieniasz, P. D. (2003) A bipartite late-budding domain in human immunodeficiency virus type 1. *J. Virol. 77*, 12373–12377.
7. Zhu, H., Jian, H., and Zhao, L. J. (2004) Identification of the 15FRFG domain in HIV-1 Gag p6 essential for Vpr packaging into the virion. *Retrovirology 21*, 1:26.
8. Barbara, M., Tilo, P., and Hans-Georg, K. (2002) The Late-Domain-Containing Protein p6 Is the Predominant Phosphoprotein of Human Immunodeficiency Virus Type 1 Particles. *J. Virol. 76*, 1015–1020.
9. Ott, D. E., Chertova, E. N., Busch, L. K., Coren, L. V., Gagliardi, T. D., and Johnson, D. G. (1999) Mutational Analysis of the Hydrophobic Tail of the Human Immunodeficiency Virus Type 1 $p6^{Gag}$ Protein Produces a Mutant That Fails To Package Its Envelope Protein. *J. Virol. 73*, 19–24.
10. Siddhartha, A. K., Zhao, Z., Clark, P. K., Tarasov, S., Alexandratos, J. N., Campbell, S. J., Kvaratskhelia, M., Lebowitz, J., and Rein, A. (2007) Interactions between HIV-1 Gag molecules in solution: An inositol phosphate-mediated switch. *J. Mol. Biol. 365*, 799–811.
11. Strack, B., Calistri, A., Craig, S., Popova, E., and Göttlinger, H. G. (2003) AIP1/ALIX is a binding partner for HIV-1 p6 and EIAV p9 functioning in virus budding. *Cell 114*, 689–699.
12. Rouzic, E. L., and Benichou, S. (2005) The Vpr protein from HIV-1: Distinct roles along the viral life cycle. *Retrovirology 22*, 2–11.
13. Freed, E. O. (2001) HIV-1 replication. *Somatic Cell Mol. Genet. 26*, 13–33.
14. Mairea, M., Champeila, P., and Møller, J. V. (2000) Interaction of membrane proteins and lipids with solubilizing detergents. *Biochim. Biophys. Acta 1508*, 86–111.
15. Schievano, E., Calisti, T., Menegazzo, I., Battistutta, R., Peggion, E., Mammi, S., Palù, G., and Loregian, A. (2004) pH-Dependent conformational changes and topology of a herpesvirus translocating peptide in a membrane-mimetic environment. *Biochemistry 43*, 9343–9351.
16. Ruan, K. H., Li, D., Ji, J., Lin, Y. Z., and Gao, X. (1998) Structural characterization and topology of the second potential membrane anchor region in the thromboxane A2 synthase amino-terminal domain. *Biochemistry 37*, 822–830.
17. Li, Y., Han, X., Bushweller, J. H., Cafiso, D. S., and Tamm, L. K. (2005) Membrane structures of the hemifusion-inducing fusion peptide mutant G1S and the fusion-blocking mutant G1V of influenza virus hemagglutinin suggest a mechanism for pore opening in membrane fusion. *J. Virol. 79*, 12065–12076.
18. Hwang, P. M., Choy, W. Y., Lo, E. I., Chen, L., Forman-Kay, J. D., Raetz, C. R., Privé, G. G., Bishop, R. E., and Kay, L. E. (2002) Solution structure and dynamics of the outer membrane enzyme PagP by NMR. *Proc. Natl. Acad. Sci. U.S.A. 99*, 13560–13565.
19. Wagner, G., Kumar, A., and Wuthrich, K. (1981) Systematic application of two-dimensional ^{1}H nuclear-magnetic-resonance techniques for studies of proteins. 2. Combined use of correlated spectroscopy and nuclear Overhauser spectroscopy for sequential assignments of backbone resonances and elucidation of polypeptide secondary structures. *Eur. J. Biochem. 114*, 375–384.
20. Wuthrich, K., Wider, G., Wagner, G., and Braun, W. (1982) Sequential resonance assignments as a basis for determination of spatial protein structures by high resolution proton nuclear magnetic resonance. *J. Mol. Biol. 155*, 311–319.
21. Wagner, G., and Wüthrich, K. (1982) Sequential resonance assignments in protein ^{1}H nuclear magnetic resonance spectra. Basic pancreatic trypsin inhibitor. *J. Mol. Biol. 155*, 347–366.
22. Wuthrich, K. (1986) *NMR of Proteins and Nucleic Acids*, Wiley, New York.
23. Piotto, M., Daudek, V., and Sklenar, V. (1992) Gradient-tailored excitation for single-quantum NMR spectroscopy of aqueous solutions. *J. Biomol. NMR 2*, 661–665.
24. Braunschweiler, L., and Ernst, R. R. (1983) Coherence Transfer by Isotropic Mixing: Application to Proton Correlation Spectroscopy. *J. Magn. Reson. 53*, 521–528.
25. Essmann, U., Perera, L., Berkowitz, M. L., Darden, T., Lee, H., and Pedersen, L. G. (1995) A smooth particle mesh Ewald method. *J. Chem. Phys. 103*, 8577–8593.
26. Cheng, Y., LeGall, T., Oldfield, C. J., Mueller, J. P., Van, Y. Y., Romero, P., Cortese, M. S., Uversky, V. N., and Dunker, A. K. (2006) Rational drug design via intrinsically disordered protein. *Trends Biotechnol. 24*, 435–442.
27. Dunker, A. K., Lawson, J. D., Brown, C. J., Williams, R. M., Romero, P., Oh, J. S., Oldfield, C. J., Campen, A. M., Ratliff, C. M.,

Hipps, K. W., Ausio, J., Nissen, M. S., Reeves, R., Kang, C., Kissinger, C. R., Bailey, R. W., Griswold, M. D., Chiu, W., Garner, E. C., and Obradovic, Z. (2001) Intrinsically disordered protein. *J. Mol. Graphics Modell. 19*, 26–59.
28. Seelig, J. (2004) Thermodynamics of lipid-peptide interactions. *Biochim. Biophys. Acta 1666*, 40–50.
29. Klajnert, B., Janiszewska, J., Urbanczyk-Lipkowska, J., Bryszewska, Z., and Epand, R. M. (2006) DSC studies on interactions between low molecular mass peptide dendrimers and model lipid membranes. *Int. J. Pharm. 327*, 145–152.
30. Goddard, T. D., and Kneller, D. G. (2003) Sparky, University of California, San Francisco.
31. Fogh, R., Ionides, J., Ulrich, E., Boucher, W., Vranken, W., Linge, J. P., Habeck, M., Rieping, W., Bhat, T. N., Westbrook, J., Henrick, K., Gilliland, G., Berman, H., Thornton, J., Nilges, M., Markley, J., and Laue, E. (2002) The CCPN project: An interim report on a data model for the NMR community. *Nat. Struct. Biol. 9*, 416–418.
32. Laskowski, R. A., Rullmannn, J. A., MacArthur, M. W., Kaptein, R., and Thornton, J. M. (1996) AQUA and PROCHECK-NMR: Programs for checking the quality of protein structures solved by NMR. *J. Biomol. NMR 8*, 477–486.
33. Clore, G. M., and Gronenborn, A. M. (1994) Multidimensional heteronuclear nuclear magnetic resonance of proteins. *Methods Enzymol. 239*, 349–363.
34. Brooks, B. R., Bruccoleri, R. E., Olafson, B. D., States, D. J., Swaminathan, S., and Karplus, M. (1983) CHARMM: A program for macromolecular energy, minimization, and dynamics calculations. *J. Comput. Chem. 4*, 187–217.
35. Gumbart, J., Wang, Y., Aksimentiev, A., Tajkhorshid, E., and Schulten, K. (2005) Molecular dynamics simulations of proteins in lipid bilayers. *Curr. Opin. Struct. Biol. 15*, 423–431.
36. Fossen, T., Wray, V., Bruns, K., Rachmat, J., Henklein, P., Tessmer, U., Maczurek, A., Klinger, P., and Schubert, U. (2005) Solution structure of the human immunodeficiency virus type 1 p6 protein. *J. Biol. Chem. 280*, 42515–42527.
37. Dyson, H. J., and Wright, P. E. (2001) Nuclear magnetic resonance methods for elucidation of structure and dynamics in disordered states. *Methods Enzymol. 339*, 258–270.
38. Lu, Y. L., Bennett, R. P., Wills, J. W., Gorelick, R., and Ratner, L. (1995) A leucine triplet repeat sequence (LXX)4 in p6gag is important for Vpr incorporation into human immunodeficiency virus type 1 particles. *J. Virol. 69*, 6873–6879.
39. Munshi, U. M., Kim, J., Nagashima, K., Hurley, J. H., and Freed, E. O. (2007) An Alix fragment potently inhibits HIV-1 budding: Characterization of binding to retroviral YPXL late domains. *J. Biol. Chem. 282*, 3847–3855.
40. Linge, J. P., Habeck, M., Rieping, W., and Nilges, M. (2003) ARIA: Automated NOE assignment and NMR structure calculation. *Bioinformatics 19*, 315–316.
41. Klauda, J. B., Brooks, B. R., MacKerell, A. D., Venable, R. M., and Pastor, R. W. (2005) An ab Initio Study on the Torsional Surface of Alkanes and Its Effect on Molecular Simulations of Alkanes and a DPPC Bilayer. *J. Phys. Chem. B 109*, 5300–5531.
42. Gunasekaran, K., Tsai, C., Kumar, S., Zanuy, D., and Nussinov, R. (2003) Extended disordered proteins: Targeting function with less scaffold. *Trends Biochem. Sci. 28*, 81–85.
43. Roccatano, D., Colombo, G., Fioroni, M., and Mark, A. E. (2002) Mechanism by which 2,2,2-trifluoroethanol/water mixtures stabilize secondary-structure formation in peptides: A molecular dynamics study. *Proc. Natl. Acad. Sci. U.S.A. 99*, 12179–12184.
44. Lee, S., Joshi, A., Nagashima, K., Freed, E. O., and Hurley, J. H. (2007) Structural basis for viral late-domain binding to Alix. *Nat. Struct. Mol. Biol. 14*, 194–199.
45. Votteler, J., Studtrucker, N., Sörgel, S., Münch, J., Rücker, E., Kirchhoff, F., Schick, B., Henklein, P., Fossen, T., Bruns, K., Sharma, A., Wray, V., and Schubert, U. (2007) Proline 35 of Human Immunodeficiency Virus Type 1 (HIV-1) Vpr Regulates the Integrity of the N-Terminal Helix and the Incorporation of Vpr into Virus Particles and Supports the Replication of R5-Tropic HIV-1 in Human Lymphoid Tissue Ex Vivo. *J. Virol. 81* (17), 9572–9576.
46. Engler, A., Stangler, T., and Willbold, D. (2003) Solution structure of human immunodeficiency virus type 1 Vpr(13−33) peptide in micelles. *Eur. J. Biochem. 268*, 389–395.
47. Schüler, W., Wecker, K., Rocquigny, H., Baudat, Y., Sire, J., and Roques, B. P. (1999) NMR structure of the (52−96) C-terminal domain of the HIV-1 regulatory protein Vpr: Molecular insights into its biological functions. *J. Mol. Biol. 285*, 2105–2117.
48. Ebbets-Reed, D., Scarlata, S., and Carter, C. A. (1996) The major homology region of the HIV-1 gag precursor influences membrane affinity. *Biochemistry 35*, 14268–14275.
49. Bouamr, F., Scarlata, S., and Carter, C. A. (2003) Role of myristylation in HIV-1 Gag assembly. *Biochemistry 42*, 6408–6417.
50. Ott, D. E. (2008) Cellular proteins detected in HIV-1. *Rev. Med. Virol. 18*, 159–175.
51. Stys, D., Blaha, I., and Strop, P. (1993) Structural and functional studies on the p6 protein from HIV-1 *gag* open reading frame. *Biochim. Biophys. Acta 1182*, 157–161.
52. Morellet, N., Bouaziz, S., Petitjean, P., and Roques, B. P. (2003) NMR structure of the HIV-1 regulatory protein VPR. *J. Mol. Biol. 327*, 215–227.

BI801794V